Impact of Noise and Complexity on Targeted Image Steganalysis

Hassan Imani
Security Analysis Laboratory
Tehran, Iran
imani@salab.ir

Mohammad Rezaei
Security Analysis Laboratory
Tehran, Iran
rezaei@salab.ir

***Abstract*— The changes made by steganography to an image can be considered as noise addition. A fundamental question is how well targeted steganalytic methods distinguish between the stego signal and naturally occurring noise in images. Moreover, several researchers have proposed steganographic methods that hide the message data in the complex regions of images. They argue that those regions are more secure for data hiding. However, no systematic experiments, to the best of our knowledge, have been presented to confirm the claims. This paper provides an experimental study to answer the questions about the impact of noise and complexity on the performance of targeted steganalytic methods. Three well-known targeted steganalytic methods are tested when spatial domain steganography is considered. Three types of noise at different levels are added to images, and two groups of complex and non-complex images are considered. Our experiments show a significant decrease in the detection accuracy of all the selected steganalytic methods for complex images. The methods demonstrate different responses to different noise types. Their performance degrades the most by Gaussian, and the least by salt & pepper noise.**

Keywords— steganography, steganalysis, data hiding, targeted, noise, complexity

I. Introduction

Least Significant Bit (LSB) is arguably the most widely used hiding technique, and the most notable method in the stego community. Accordingly, many *targeted* and *universal* steganalytic methods have been introduced to detect the LSB-based methods [1]. Targeted or specific steganalytic methods, which construct features for a known steganographic method, provide more accurate results than universal or blind methods [2]. High accuracy of many targeted methods have been reported in research papers [3]. However, the effect of *noise* and *complexity* of cover images are not considered. In order to make steganalysis difficult, several steganographic methods have been designed to pretend the stego data as natural additive noise, and several others hide data in complex regions of the image. A question is how well a targeted method performs for given cover images which are naturally noisy or complex. More specifically, how increasing noise and complexity may affect the performance of a targeted steganalytic method.

Data embedding, in several works such as LSB *matching* [4] and *stochastic modulation steganography* [5], is modeled as noise addition in order to simulate the stego data as a natural noise. The reason is that there are naturally several sources of noise in capturing and transmitting the image, such as quantization, sensor, and channel. Digital camera or scanner produce images with some degree of noise that is helpful for steganography, because the changes from embedding data are masked. However, modern steganalytic methods claim that they can distinguish between natural noisy and stego images. The main reason is that the natural noise is added before quantization of the signal in the A/D converter, and a number of processes such as demosaicking, color correction, and filtering are applied before the final image is acquired [6]. Nevertheless, there are studies that show the presence of noise affects the performance of the steganalytic methods [6, 7].

Complexity of images is another important factor that affects the performance of steganalytic methods [7]. The main hypothesis is that complex images or complex regions in images are more secure for embedding data. One reason is that *human visual system* (HVS) is less sensitive to changes in complex regions with a lot of edges than smooth regions [7]. A good steganalysis system should distinguish cover and stego images with different complexities.

In this paper, we conduct an experimental study on the effect of noise and complexity on the performance of selected well-known targeted steganalytic methods including *regular/singular* (RS), *sample pair analysis* (SPA), and *Chi-square* attack. To explore the effect of noise, three common types of noise at 10 *signal-to-noise* (SNR) ratios are added to the images, and to study the effect of complexity, complex and non-complex images are selected from an image database based on two image complexity metrics. Our study shows that all types of noise degrade the performance of the steganalytic methods, however, Gaussian and speckle noises have a more severe impact. Furthermore, the steganalytic methods provide significantly less accurate results for complex images comparing with non-complex ones.

II. Methods

A. Targeted Steganalysis Methods

Targeted steganalytic methods construct features for a known steganographic method and therefore, may work well only for that method. We select three well-known methods to evaluate the impact of noise and complexity on their

978-1-5386-5538-2/18/$31.00 ©2018 IEEE

performance: Chi-square, RS, and SPA. In the following, a short description of each method is presented.

1) Chi-square Attack.

Chi-square attack is the most notable early targeted method that can detect LSB-replacement steganography if the message is embedded sequentially. However, it was later generalized to detect randomly distributed messages [8]. This attack analyzes pairs of values, in the histogram, that are swapped during LSB replacement. Binary representations of a pair of values $2n$ and $2n+1$ differ only in the LSB. After LSB embedding, the occurrences of values $2n$ and $2n+1$ denoted by O_{2n} and O_{2n+1} will be equal if the message bits are equally distributed. The sum $O_{2n}+O_{2n+1}$ will be the same before and after embedding, and therefore, the average of O_{2n} and O_{2n+1} is the same for both the cover and stego images:

$$O_{2n}^{e} = \frac{O_{2n} + O_{2n+1}}{2} \tag{1}$$

The expected value O_{2n}^{e} can therefore be calculated from the stego image. Chi-square attack measures the statistical significance that the occurrences of two values in each pair is equal. It performs this by comparing the expected value O_{2n}^{e} with O_{2n}, which is calculated from the stego image [9]. The χ^2 statistic is given as:

$$\chi_{k-1}^{2} = \sum_{n=1}^{k} \frac{(O_{2n} + O_{2n}^{e})}{O_{2n}^{e}} \tag{2}$$

with k-1 degrees of freedom, where k is the number of pairs of values. The probability of embedding is derived by integration of the density function as follows:

$$p = 1 - \frac{1}{2^{\frac{k-1}{2}}\Gamma\left(\frac{k-1}{2}\right)} \int_{0}^{\chi_{k-1}^{2}} e^{-\frac{x}{2}} x^{\frac{k-1}{2}-1} dx \tag{3}$$

where $\Gamma(.)$ is the Euler Gamma function.

2) Regular/Singular (RS) Attack.

There is a natural correlation between the neighboring pixels in a cover image. LSB embedding disturbs this correlation.

The idea of RS attack [10] is to intentionally modify the LSBs of a given image, and inspect if the correlation increases or decreases. The hypothesis is that the correlation decreases for the stego and increases for the cover image. The correlation between a group of adjacent pixels is evaluated by a discrimination function f, which calculates the sum of absolute differences. Modifying the LSBs of the group is performed by a flipping permutation operation F. Suppose a group G of 4 neighboring pixels. It will belong to one of the three categories:

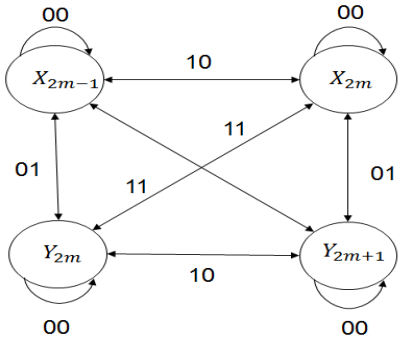

Fig. 1. Finite state machine that describes the transitions between multisets.

- Regular groups: $G \in R \leftrightarrow f\left(F(G)\right) > f(G)$
- Singular groups: $G \in S \leftrightarrow f\left(F(G)\right) < f(G)$
- Unusable groups: $G \in U \leftrightarrow f\left(F(G)\right) = f(G)$

Flipping operation somehow simulates the LSB embedding process, and therefore, it is like the embedding is performed twice for a stego image. This can restore the original intensities of the pixels and increase the correlations. Thus, the expected number of S groups for the stego image is smaller comparing to the cover image.

Different flipping can be applied to different pixels. This is performed using a mask M, for example [1 0 0 1] for a group of 4 pixels. We denote the number of groups R and S for mask M by RM and SM, and that for mask $-M$ by R-M and S-M. Fridrich observed that $RM \approx R\text{-}M$ and SM≈S-M for a cover image however, this balance is disturbed by LSB embedding to some degree proportional to length of the stego data [10].

3) Sample Pair Analysis (SPA)

This technique uses the statistical properties of neighboring pixels, which are very sensitive to LSB embedding. Considering two adjacent pixels called *sample pair*, higher order statistics such as local correlation is utilized.

All the sample pairs are grouped in several multisets. Consider an 8-bit grayscale image. The multiset D_n, $0 \le n \le 255$ include the sample pairs for which the difference between two values in the pair is n. C_m, $0 \le m \le 127$ denotes the multiset that include the sample pairs whose 7 first bits differ by m. C_m remains unchanged under LSB embedding. It can be simply shown that $D_{2m} \subset C_m$ but D_{2m+1} is shared between C_m and C_{m+1}. The pairs in D_{2m+1} with larger even value construct the multiset X_{2m+1}, and the pairs with larger odd value construct the multiset Y_{2m+1}. For a natural image, we have [3]:

$$\left|\{Y_{2m+1}\}\right| = \left|\{X_{2m+1}\}\right| \tag{4}$$

LSB embedding disturbs this equality. The multiset C_m which is closed under LSB embedding can be partitioned into $X_{2m\text{-}1}$, D_{2m}, and Y_{2m+1}. Two more multisets are defined by partitioning D_{2m}: X_{2m} includes the pairs of the form $(2k\text{-}2m, 2k)$ and $(2k+1, 2k\text{-}2m+1)$ and Y_{2m} consists of the pairs of the form $(2k\text{-}2m+1, 2k+1)$ and $(2k, 2k\text{-}2m)$. The reason for these

definitions is that the multisets X_{2m-1}, X_{2m}, Y_{2m}, and Y_{2m+1} are converted to each other under LSB embedding, and the changes can be modeled by a finite state machine as shown in Fig. 1. The value 01 in the figure indicates that the LSB of first value in the sample pair remains unchanged and the LSB of the second value is reversed.

The probabilities of transitions between the multisets are known. Accordingly, the size of each multiset can be estimated before and after embedding. A set of quadratic equations for different m are finally derived by which the embedding rate β can be approximated:

$$\frac{\left(|C_m|-|C_{m+1}|\right)\beta^2}{4}+|Y_{2m+1}|-|X_{2m+1}|-\frac{\left(|D_{2m}|-|D_{2m+2}|+2|Y_{2m+1}|-2|X_{2m+1}|\right)\beta}{2}=0 \tag{5}$$

The smallest root of (5) is considered.

B. Noise

Image noise, which is undesirable random changes in the values of pixels, is produced during image acquisition, transmission, etc. [11]. Acquisition noise is mainly produced in the sensor of the imaging device. The sensor noise is usually categorized into three categories: *fixed pattern noise*, *banding noise*, and *random noise* [12, 13].

Fixed pattern noise is originated from unevenness of sensors during manufacturing. It usually happens during longer exposure shots, when some pixels are more sensitive to light. Banding noise is generated when reading the data from the digital sensor using A/D convertors. This type of noise is more noticeable at high speed, and in shadows, or in excessive light. Fixed pattern and banding noise are highly deterministic and predictable, and can be reduced by advanced manufacturing and signal processing techniques. The third category is random noise, which is mainly caused by photon emission, photoelectric effects, dark current, and thermal noise. Dark current and thermal noise have been significantly reduced by hardware improvements, but photon emission and photoelectric effects cannot be removed [12]. In our experimental study, we select two common noise types including Gaussian and salt & pepper, which are additive noise and produced during image acquisition by digital cameras. We also consider speckle noise, which is a multiplicative noise [14, 15].

Gaussian noise, caused by thermal noise, is independent at each pixel, and independent of the signal intensity. Its probability density function is same as the normal distribution [14, 16]. The mathematical model can be written as [14]:

$$g(i,j)=f(i,j)+n(i,j) \tag{6}$$

where $1\le i\le H$ and $1\le j\le W$, and H and W represent the size of the image.

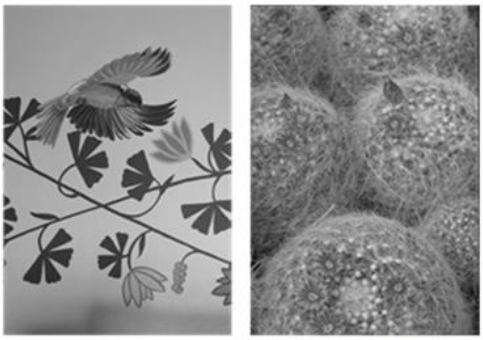

Fig. 2. Image complexity measures: the shape parameter of GGD and bit-plane based complexity.

An image with salt & pepper (also called impulsive, or spike) noise has bright pixels in darker regions and dark pixels in brighter regions [17]. This noise is produced by several sources such as errors in A/D convertor and errors transmission [18]. The mathematical model can be written as [14]:

$$g(i,j)=\begin{cases} h_j & \textit{with probability } h \\ f_j & \textit{with probability } 1-h \end{cases} \tag{7}$$

where f_j is the pixel value of the image f at location (i, j), h_j is random number, and h is the noise ratio.

Speckle noise is a granular pattern, which is inherent property of medical ultrasound, optical coherent tomography, active radar, and *synthetic aperture radar* (SAR) images. Its mathematical model is as follows [14]:

$$g(i,j)=f(i,j)*n(i,j) \tag{8}$$

C. Complexity

There is no standard definition for image complexity. A rough definition might be as background uniformity and foreground clutter. Several measures have been proposed in different fields to assess image complexity [19-22]. Two common measures include the shape parameter of the *generalized Gaussian distribution* (GGD) [23], and *bit-plane based complexity* [24].

1) The Shape Parameter of GGD

Liu [23] uses a complexity measure that is a PDF approximation of the marginal density of coefficients at high-pass sub-bands in wavelet domain. A good approximation is obtained if the parameters of GGD are adaptively being varied. The PDF is defined as:

$$p(x;\alpha,\beta)=\frac{\beta}{2\alpha\Gamma(1/\beta)}e^{-(|x|/\alpha)^{\beta}} \tag{9}$$

where $\Gamma(.)$, α and β are Gamma function, scale parameter, and shape parameter, respectively.

The shape parameter β can be considered as a measure of complexity, where a larger β indicates higher complexity. Fig. 2 shows two grayscale images whose complexities are well represented by β value.

2) Bit-Plane Based Complexity

This measure of complexity is used in bit-plane complexity segmentation (BPCS) steganography [24]. An 8-bit grayscale image is divided into 8 binary images called bit-planes, and the complexity is derived for each binary image. For a single bit-plane of the size $H \times W$, the number of changes in adjacent pixels from zero to one, and vice versa is calculated as n. The resulting value is then normalized by the maximum possible number of changes, which is equal to $(H\text{-}1)\times(W\text{-}1)$ as follows:

$$\alpha_{BPCS} = \frac{n}{(H-1)(W-1)} \tag{10}$$

We estimate the overall complexity of the grayscale image by averaging the complexity values of the bit-planes. Fig. 2 shows the complexity value for two images with different complexity levels.

III. Experiments

We evaluate the performance of three targeted steganalytic methods including Chi-square, RS, and SPA in presence of noise and complex images. Chi-square is a targeted attack for detecting sequentially embedded message, and in our experiments we tested this method only for sequential stego images, while both RS and SPA are used for detecting randomly scattered message in the images.

Gaussian, salt & pepper, and speckle noise are added to images, and two sets of complex and non-complex images are considered, which are chosen according to two complexity measures: the shape parameter of GGD and bit-plane based complexity.

A. Dataset

We used our GSC1_BMP_Gray dataset which consists of 2000 cover images. The original images of this dataset were selected from Greenspun website[1]. However, they needed a few processes such as cropping the black border around images. Fig. 3 shows the procedure to select 100 complex and 100 non-complex images from the dataset, and produce noisy and stego versions. To select complex and non-complex images, we calculated the two complexity measures for all the images in the dataset. Top 100 complex images were selected according to the agreement of both measures, and 100 non-complex images were chosen in the same way.

Three types of noise, each with 10 SNR levels, were added to the 100 non-complex images, resulting in 3000 noisy images. The amount of image noise is doubled in each subsequent level. Two LSB embedding methods including *sequential* and *random LSB replacement* (SLSBR and RLSBR) were then applied to generate stego images with four embedding rates (0.05, 0.1, 0.2, and 0.5) for complex and non-complex, and one embedding rate (0.05) for noisy images. In total, 3200 cover and 7600 stego images are available for the experiments. The SLSBR method is used for evaluating Chi-square attack, and RLSBR for SPA and RS attacks.

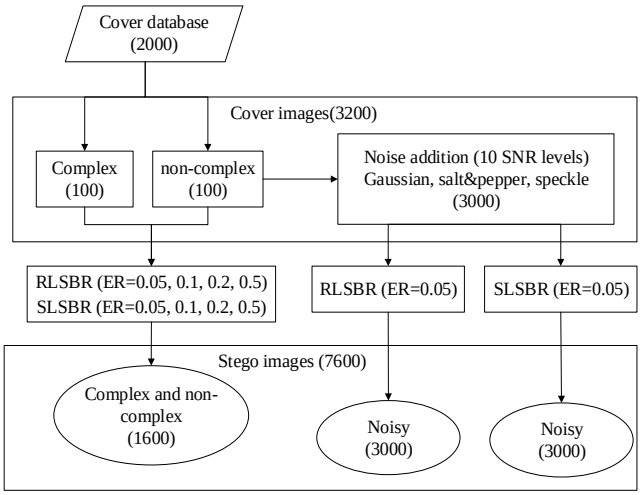

Fig. 3. The dataset containing complex, non-complex, and noisy cover images, and their stego versions. ER: Embedding Rate.

B. Impact of Complexity

The results of three targeted steganalytic methods on complex and non-complex images are reported in Tables I and II. The false positive (FP) rate of all methods is more than 0.5 for complex images, while it is almost zero for non-complex ones. These results demonstrate the unreliability of the selected targeted methods when analyzing complex cover images. In general, accuracy and precision improve by increasing the embedding rate, however, they are significantly larger for non-complex images. Fig. 4 better illustrates the comparison of the detection accuracy for complex and non-complex images as the embedding rate increases. It can also be seen that RS performs slightly better than SPA for complex, while SPA provides a better detection accuracy for non-complex stego images. We have tuned the threshold of Chi-square attack equal to 0.03 to have low FP and high true positive (TP) rates for non-complex images. This results in very high FP rate for complex images, see Table II. Increasing the threshold can improve the results for complex images but it degrades the good results for non-complex images.

C. Impact of Noise

In this experiment, we consider stego images with the embedding rate 0.05, and set the thresholds for SPA, Chi-square, and RS to 0.045, 0.03, and 0.04, respectively. Figs 5, 6, and 7 show the FP, TP, and accuracy rates of the steganalytic methods for different noise levels from 0 to 10. The noise level 0 is associated with the original noise-free images. The results suggest the following conclusions:

[1] http://philip.greenspun.com/photography

TABLE I. STEGANALYSIS RESULTS FOR NON-COMPLEX IMAGES.

	RS				Chi-square				SPA			
ER	0.05	0.1	0.2	0.5	0.05	0.1	0.2	0.5	0.05	0.1	0.2	0.5
Accuracy	0.91	0.96	0.99	1	0.87	0.90	0.93	0.95	0.98	0.99	0.99	0.99
Precision	1	1	1	1	0.90	0.91	0.91	0.92	0.99	1	1	1
FP rate	0	0	0	0	0.09	0.09	0.09	0.09	0.02	0.02	0.02	0.02
TP rate	0.83	0.93	0.98	1	0.83	0.9	0.96	0.99	0.99	1	1	1

TABLE II. STEGANALYSIS RESULTS FOR COMPLEX IMAGES.

	RS				Chi-square				SPA			
ER	0.05	0.1	0.2	0.5	0.05	0.1	0.2	0.5	0.05	0.1	0.2	0.5
Accuracy	0.60	0.66	0.72	0.72	0.52	0.52	0.52	0.52	0.6	0.65	0.7	0.73
Precision	0.58	0.61	0.64	0.64	0.51	0.51	0.51	0.51	0.58	0.61	0.64	0.65
FP rate	0.55	0.55	0.55	0.55	0.97	0.97	0.97	0.97	0.53	0.53	0.53	0.53
TP rate	0.76	0.88	0.99	0.99	1	1	1	1	0.71	0.81	0.91	0.98

- For SPA, the FP rate increases with the noise level for all noise types. However, SPA is affected by salt & pepper noise much less than Gaussian and Speckle noise. The TP rate also increases with the noise level for Gaussian and speckle noise, but it is not affected by the salt & pepper noise. Besides, the accuracy of SPA decreases as the noise level increases, however, the decrease is much more significant for Gaussian and speckle than salt & pepper.
- Chi-square and RS attacks show a different behavior than SPA in terms of FP rate. Surprisingly, the FP rate decreases after a certain noise level for Gaussian and speckle noise.
- Chi-square is not affected by salt & pepper noise in both terms of FP and TP rates. There can be seen even a decrease in the FP rate and an increase in the TP rate, resulting a better accuracy. After the noise level 3, the FP rate starts to decrease, and consequently, the accuracy starts to increase until the noise level 9. The results at the noise level 10 seem unusual. The reason might be that the image is too noisy that no local correlations exist anymore. The speckle noise shows a different impact than Gaussian, where the FP rate is always (up to the noise level 9) increasing, and the accuracy decreasing.
- The impact of salt & pepper noise on the RS attack is different from SPA and Chi-square. Up to the noise level 5, the FP rate and the accuracy are quite good, but a rapid decline occurs in the performance of RS, afterwards. The sudden decrease from the noise level 9 to 10 is quite unexpected that might be because of emergence of unusual RS curves in the noise level 10 when the image is noise like. The FP rate starts decreasing after the noise level 6 both for Gaussian and speckle noise. The accuracy value 0.5 at the noise levels larger than 5 indicates that the RS method does not work better than a random classifier.

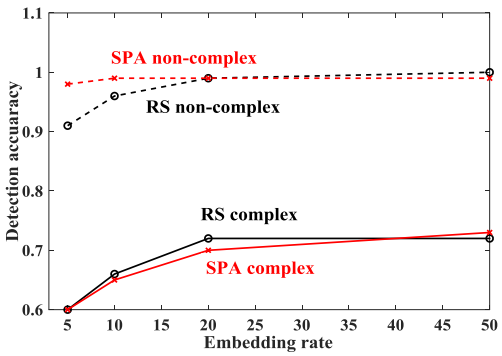

Fig. 4. The detection accuracy of RS and SPA for complex and non-complex images.

IV. CONCLUSIONS

We have conducted an experimental study on the impact of image noise and complexity on selected targeted steganalytic methods. The main goal of this work is to investigate how much the noisy or complex images without any hidden data are mistaken with stego images by the steganalytic methods. Overall, our experiments show that the performance of SPA, Chi-square, and RS steganalytic methods degrades by Gaussian and speckle noise. Chi-square, interestingly, is not affected by salt & pepper noise, while the performance of the two other methods is degraded. In the future, we plan to extend this study to other targeted and universal steganalytic methods.

REFERENCES

[1] J. Fridrich and J. Kodovský, "Steganalysis of LSB replacement using parity-aware features," in *International Workshop on Information Hiding*, 2012, pp. 31-45: Springer.

[2] B. Li, J. He, J. Huang, and Y. Q. Shi, "A survey on image steganography and steganalysis," *Journal of Information Hiding and Multimedia Signal Processing*, vol. 2, no. 2, pp. 142-172, 2011.

[3] S. Dumitrescu, X. Wu, and Z. Wang, "Detection of LSB steganography via sample pair analysis," *IEEE transactions on Signal Processing*, vol. 51, no. 7, pp. 1995-2007, 2003.

[4] T. Sharp, "An implementation of key-based digital signal steganography," in *International Workshop on Information Hiding*, 2001, pp. 13-26: Springer.

[5] J. Fridrich and M. Goljan, "Digital image steganography using stochastic modulation," in *Electronic Imaging 2003*, 2003, pp. 191-202: International Society for Optics and Photonics.

[6] J. Fridrich, *Steganography in digital media: principles, algorithms, and applications*. Cambridge University Press, 2009.

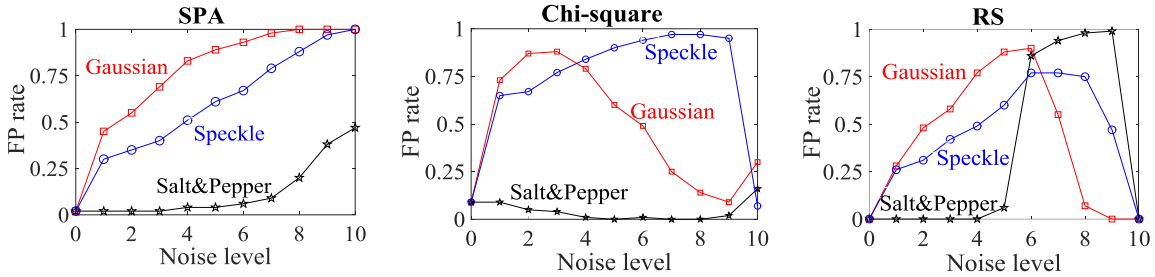

Fig. 5. FP rate for different attacks with increasing the noise level. The embedding rate for the stego images is 0.05.

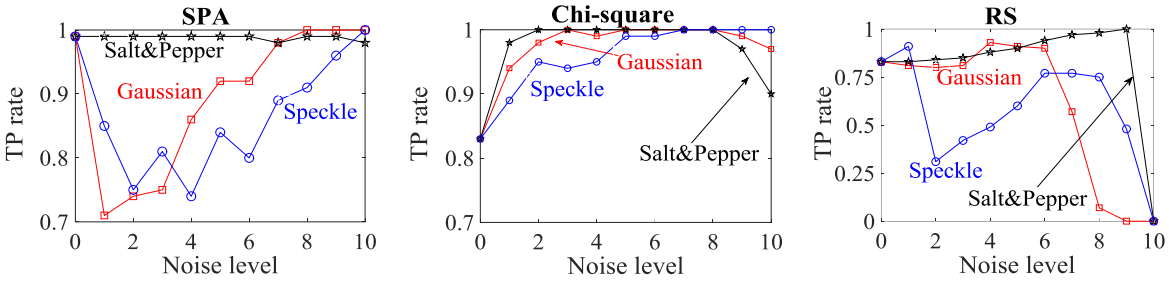

Fig. 6. TP rate for different attacks with increasing noise level. The embedding rate for the stego images is 0.05.

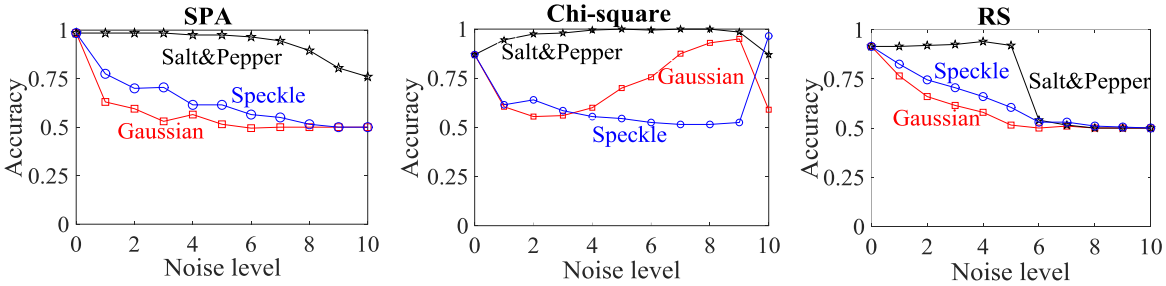

Fig. 7. Detection accuracy for different attacks with increasing noise level. The embedding rate for the stego images is 0.05.

[7] Q. Liu, A. H. Sung, B. Ribeiro, M. Wei, Z. Chen, and J. Xu, "Image complexity and feature mining for steganalysis of least significant bit matching steganography," *Information Sciences*, vol. 178, no. 1, 2008.

[8] J. Fridrich, "Feature-based steganalysis for JPEG images and its implications for future design of steganographic schemes," in *International Workshop on Information Hiding*, 2004, pp. 67-81: Springer.

[9] A. Pfitzmann, "Attacks on steganographic systems breaking the steganographic utilities EzStego Jsteg Steganos and Stools and some lessons learned," in *Workshop on Information Hiding*, 1999, pp. 1-76.

[10] J. Fridrich, M. Goljan, and R. Du, "Detecting LSB steganography in color, and gray-scale images," *IEEE multimedia*, vol. 8, no. 4, pp. 22-28, 2001.

[11] M. A. Farooque and J. S. Rohankar, "Survey on various noises and techniques for denoising the color image," *International Journal of Application or Innovation in Engineering & Management (IJAIEM)*, vol. 2, no. 11, pp. 217-221, 2013.

[12] X. Jin, Z. Xu, and K. Hirakawa, "Noise parameter estimation for Poisson corrupted images using variance stabilization transforms," *IEEE Transactions on Image Processing*, vol. 23, no. 3, pp. 1329-1339, 2014.

[13] X. Jin and K. Hirakawa, "Approximations to camera sensor noise," in *Image Processing: Algorithms and Systems*, 2013, p. 86550H.

[14] P. Vasuki, C. Bhavana, S. M. M. Roomi, and E. L. Deebikaa, "Automatic noise identification in images using moments and neural network," in *Machine Vision and Image Processing (MVIP), 2012 International Conference on*, 2012, pp. 61-64: IEEE.

[15] Y. Chen and M. Das, "An automated technique for image noise identification using a simple pattern classification approach," in *Circuits and Systems, 2007. MWSCAS 2007. 50th Midwest Symposium on*, 2007, pp. 819-822: IEEE.

[16] J. Ohta, *Smart CMOS image sensors and applications*. CRC press, 2007.

[17] A. C. Bovik, *Handbook of image and video processing*. Academic press, 2010.

[18] [18] L. G. S. G. C. Stockman, "Computer Vision," *Prentice-Hall. ISBN 0-13-030796-3*, 2001.

[19] M. P. Da Silva, V. Courboulay, and P. Estraillier, "Image complexity measure based on visual attention," in *Image Processing (ICIP), 2011 18th IEEE International Conference on*, 2011, pp. 3281-3284: IEEE.

[20] O. Le Meur, P. Le Callet, D. Barba, and D. Thoreau, "A coherent computational approach to model bottom-up visual attention," *IEEE transactions on pattern analysis and machine intelligence*, vol. 28, no. 5, pp. 802-817, 2006.

[21] L. Itti, C. Koch, and E. Niebur, "A model of saliency-based visual attention for rapid scene analysis," *IEEE Transactions on pattern analysis and machine intelligence*, vol. 20, no. 11, pp. 1254-1259, 1998.

[22] N. D. Bruce and J. K. Tsotsos, "Saliency, attention, and visual search: An information theoretic approach," *Journal of vision*, vol. 9, no. 3, pp. 5-5, 2009.

[23] Q. Liu, A. H. Sung, J. Xu, and B. M. Ribeiro, "Image complexity and feature extraction for steganalysis of LSB matching steganography," in *Pattern Recognition, 2006. ICPR 2006.* IEEE.

[24] E. Kawaguchi and R. O. Eason, "Principles and applications of BPCS steganography," in *Photonics East (ISAM, VVDC, IEMB)*, 1999, pp. 464-473: International Society for Optics and Photonics.